Akkari, Gocheva et al, Supplemental Figure 1

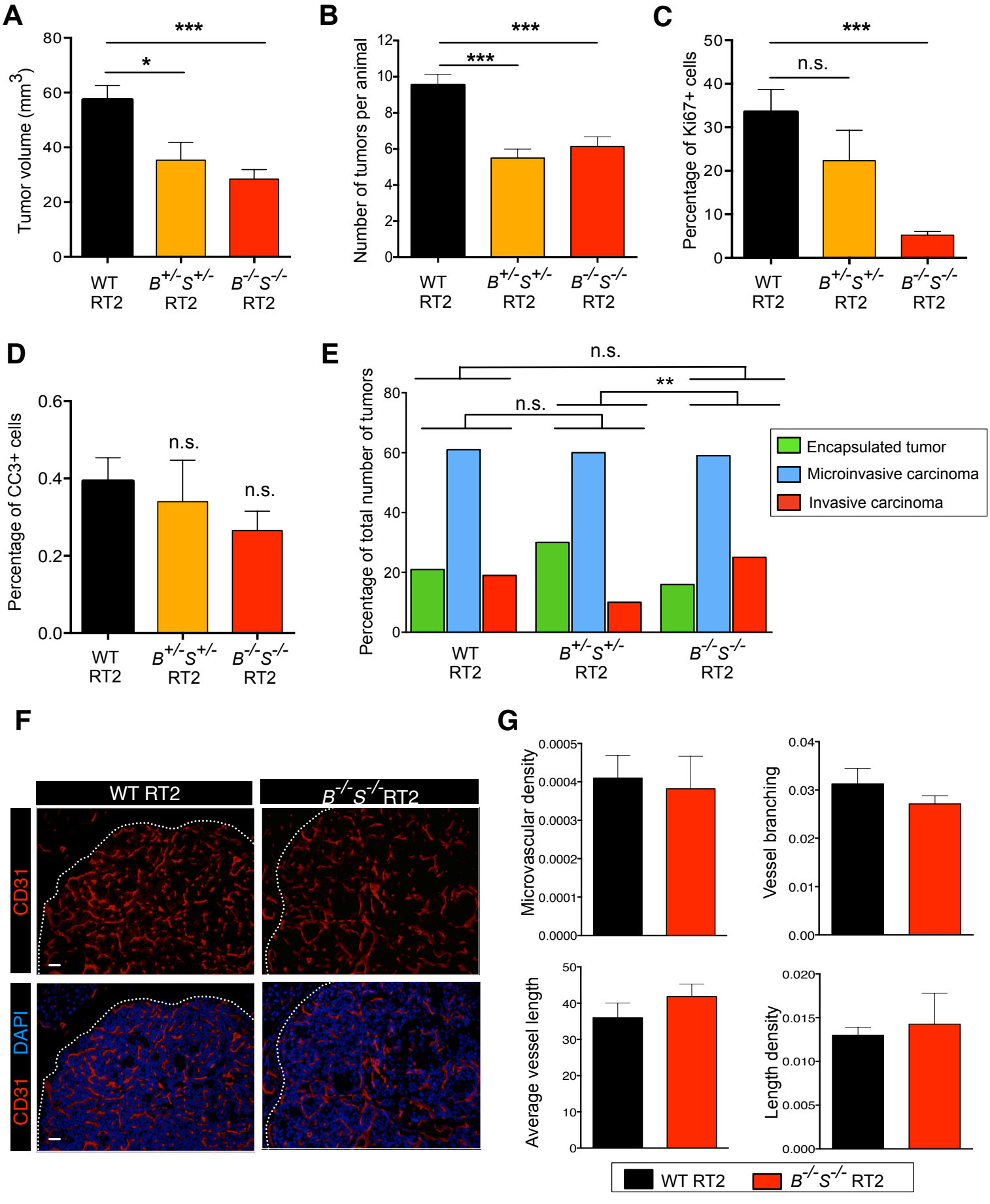

Akkari, Gocheva et al, Supplemental Figure 2

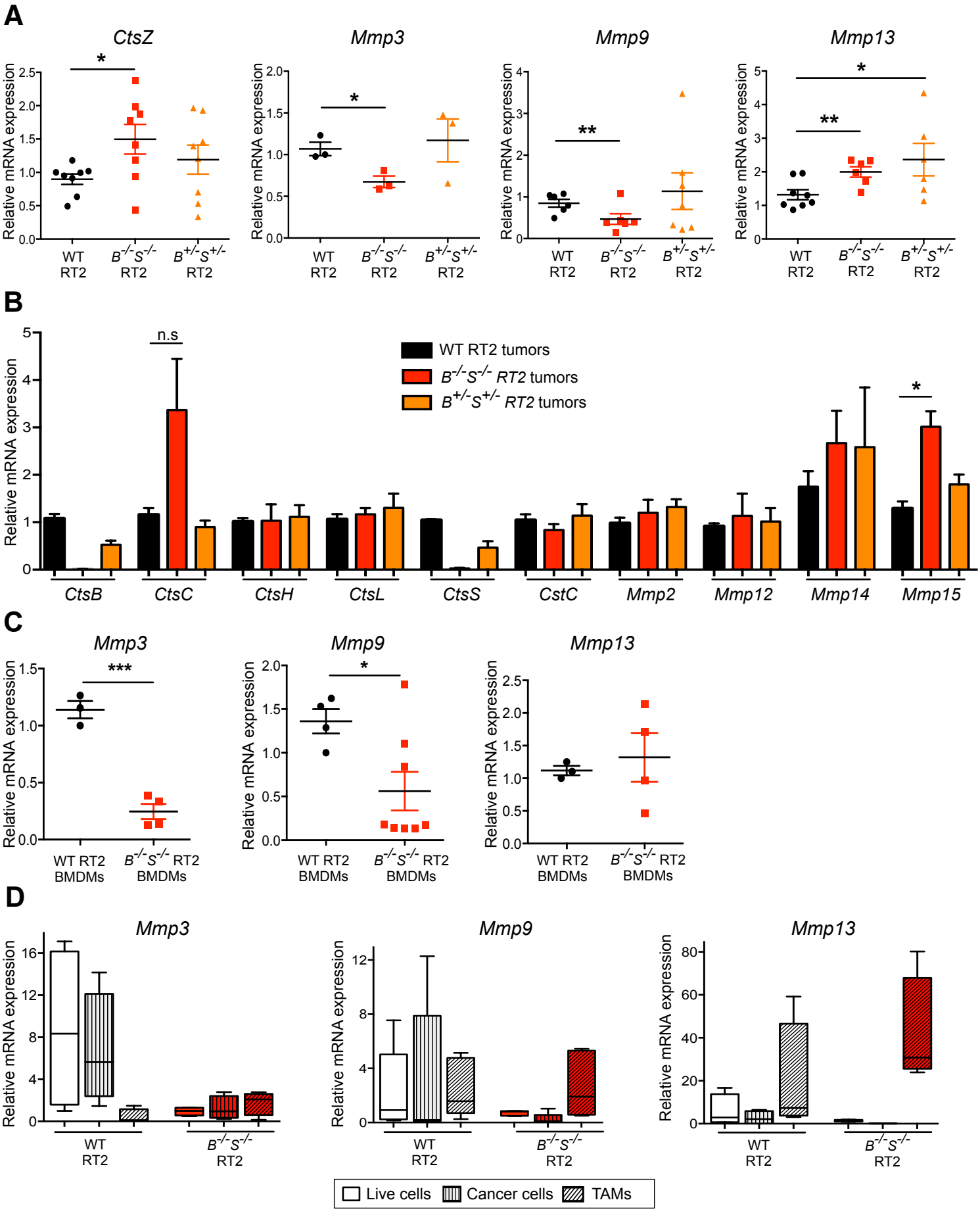

Akkari, Gocheva et al, Supplemental Figure 3

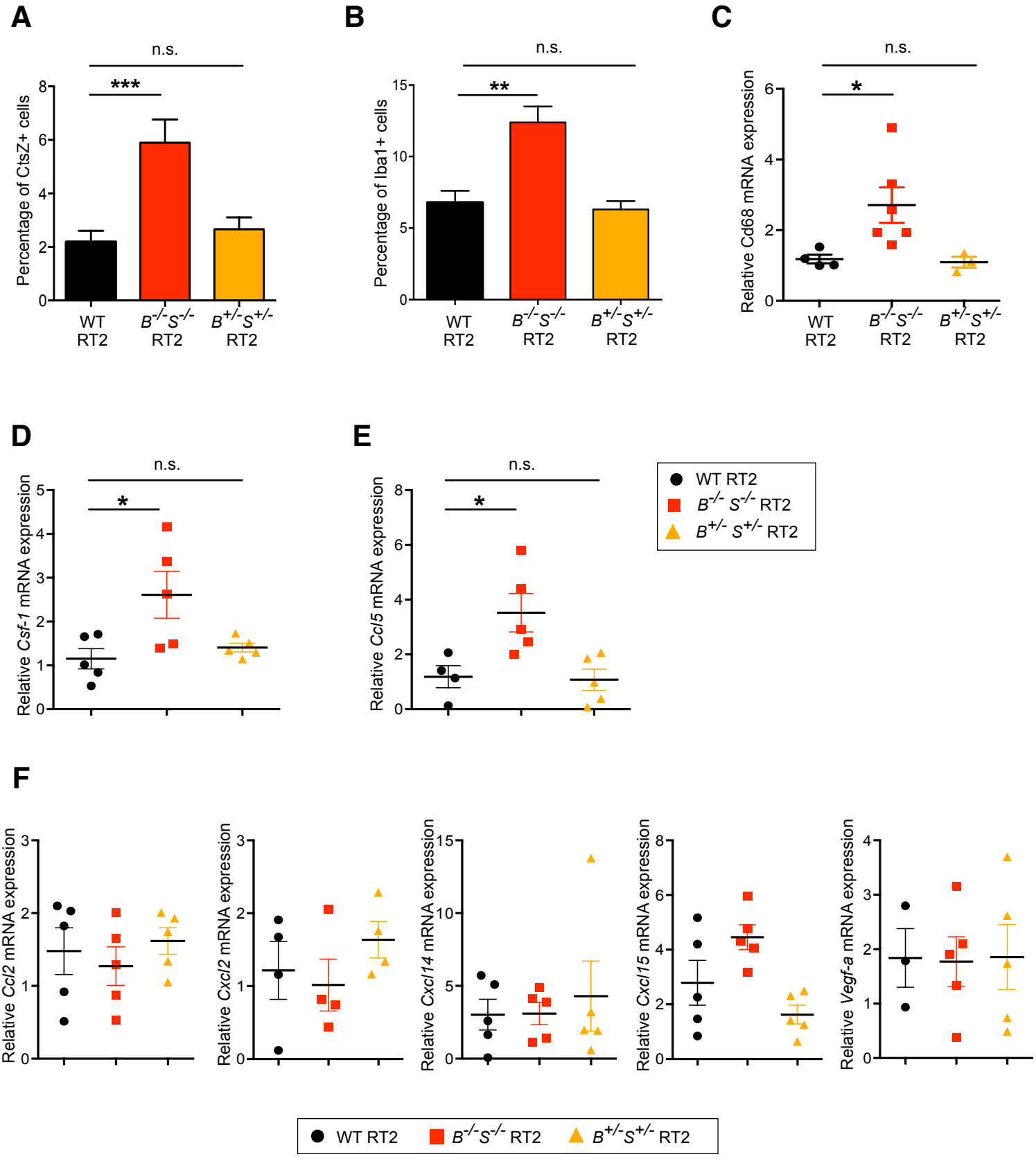

Akkari, Gocheva et al, Supplemental Figure 4

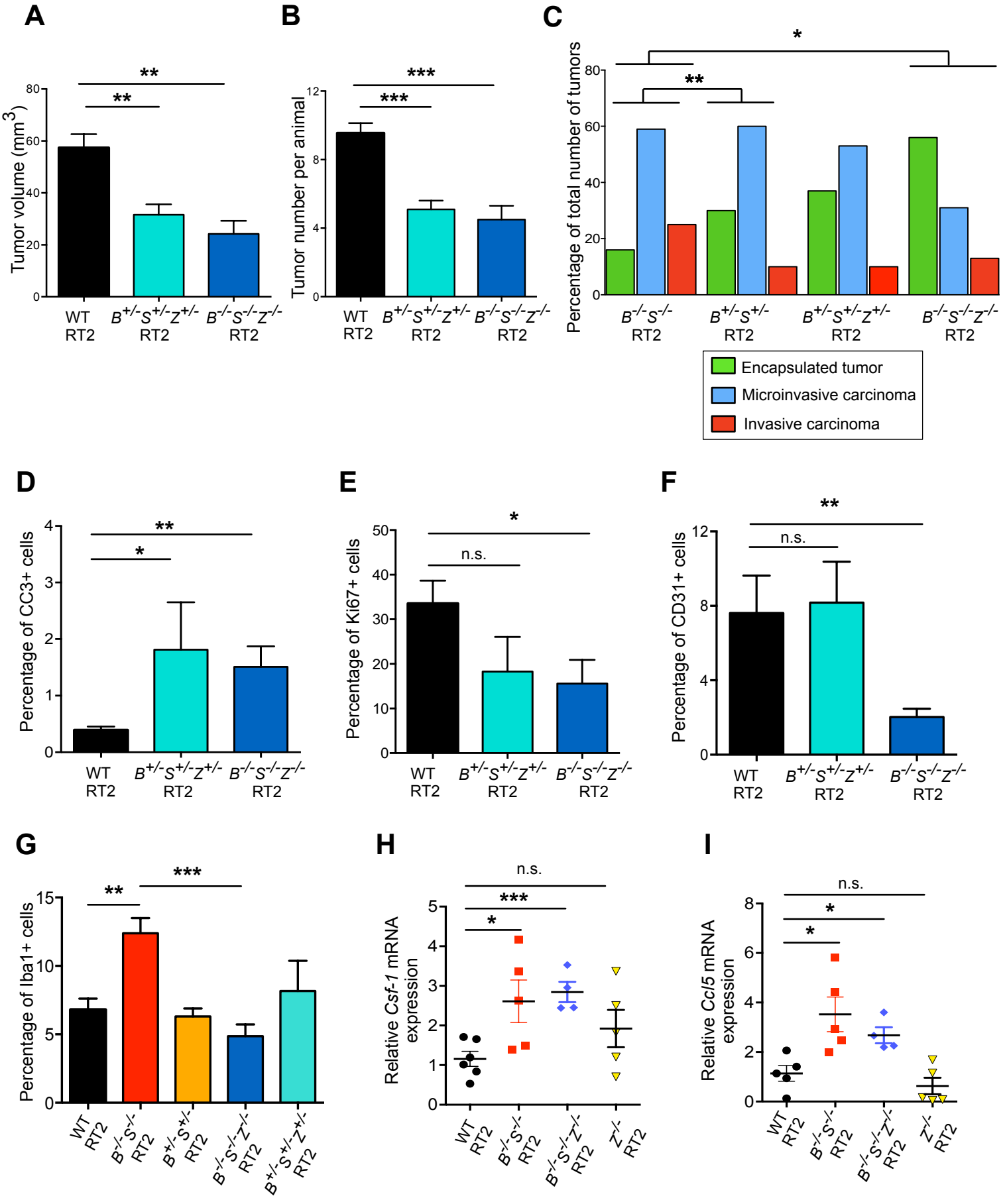

Supplemental Figure 1: Analysis of tumor burden, number, proliferation, apoptosis, invasion and vascularization in *CtsB*$^{+/-}$*S*$^{+/-}$ RT2 and *CtsB*$^{-/-}$*S*$^{-/-}$ RT2 mice.

(A) Cumulative tumor volume calculated for 13.5w WT RT2 and *CtsB*$^{-/-}$*S*$^{-/-}$ RT2 mice (as presented in Figure 1A) are plotted here with analysis of *CtsB*$^{+/-}$*S*$^{+/-}$ RT2 tumors (*n*=27), which showed a similar phenotype to that of the cathepsin double knockouts.

(B) The average number of tumors per mouse in 13.5w WT RT2 and *CtsB*$^{-/-}$*S*$^{-/-}$ RT2 animals (as presented in Figure 1B) are plotted here with the addition of *CtsB*$^{+/-}$*S*$^{+/-}$ RT2 animals (*n*=37), which showed a similar phenotype to that of the cathepsin double knockouts.

(C) Quantitation of Ki67 staining in WT and *CtsB*$^{-/-}$*S*$^{-/-}$ RT2 tumors (as presented in Figure 1D) are plotted here with analysis of proliferation in *CtsB*$^{+/-}$*S*$^{+/-}$ RT2 tumors. A significant decrease in cell proliferation was only observed for the double knockout tumors and not in the heterozygous lesions. Tumors from 5 WT RT2, 4 *CtsB*$^{+/-}$*S*$^{+/-}$ RT2, and 11 *CtsB*$^{-/-}$*S*$^{-/-}$ RT2 mice were analyzed.

(D) Quantitation of cleaved caspase-3 (CC3) staining in WT, *CtsB*$^{+/-}$*S*$^{+/-}$ and *CtsB*$^{-/-}$*S*$^{-/-}$ RT2 tumors revealed no significant changes between genotypes. Tumors from 11 WT RT2, 5 *CtsB*$^{+/-}$*S*$^{+/-}$ RT2, and 10 *CtsB*$^{-/-}$*S*$^{-/-}$ RT2 mice were analyzed.

(E) Graph showing the proportions of encapsulated, microinvasive and invasive carcinomas in WT RT2 and *CtsB*$^{-/-}$*S*$^{-/-}$ RT2 mice at 13.5w (as presented in Figure 1E) are plotted here with analysis of *CtsB*$^{+/-}$*S*$^{+/-}$ RT2 mice. The following number of tumors were graded: WT RT2: 18 mice, 97 tumors; *CtsB*$^{+/-}$*S*$^{+/-}$ RT2: 17 mice, 99 tumors; *CtsB*$^{-/-}$*S*$^{-/-}$ RT2: 14 mice, 68 tumors.

(F) Representative images of WT RT2 or *CtsB*$^{-/-}$*S*$^{-/-}$ RT2 tumors stained with the endothelial cell marker CD31 (red). The nuclei were counterstained with DAPI (blue).

(G) Detailed angiogenesis analysis did not reveal any significant difference in various blood vessel parameters between WT RT2 and *CtsB*$^{-/-}$*S*$^{-/-}$ RT2 mice. Images of tumors stained for CD31 were acquired and analyzed by manually tracing the vessels using Volocity imaging software. Five random fields per tumor

were analyzed for five mice per group. Microvascular density was calculated by dividing the number of line segments by the tumor area (top left). Vessel branching is represented by the ratio of line segments to the total vessel length (top right). The average vessel length is the total vessel length divided by the number of vessels (bottom left). Length density is calculated by dividing the total vessel length by the tumor area (bottom right).

Graphs show mean ± s.e.m. Statistical significance was calculated by unpaired two-tailed Student's t-test (A-D, G); or using a cumulative logit model with generalized estimating equations to correct for correlations within individual mice (E) (n.s.) nonsignificant, *P < 0.05, **P < 0.01, ***P < 0.001. Scale bars in (F): 50 μm.

Supplemental Figure 2: Expression analyses of multiple proteases in *CtsB*$^{+/-}$*S*$^{+/-}$ and *CtsB*$^{-/-}$*S*$^{-/-}$ tumors.

(A) mRNA expression levels of *CtsZ, Mmp3, Mmp9,* and *Mmp13* was determined by qPCR in WT RT2 and *CtsB*$^{-/-}$*S*$^{-/-}$ RT2 tumors (end-stage, 13.5w) as depicted in Figure 2A, and are plotted here with analysis of *CtsB*$^{+/-}$*S*$^{+/-}$ RT2 tumors. Other than *Mmp13* mRNA, no significant differences in mRNA expression were observed in the heterozygous *CtsB*$^{+/-}$*S*$^{+/-}$ RT2 tumors. 3-8 independent tumors per genotype were used for analysis.

(B) mRNA expression levels of *CtsB, CtsC, CtsH, CtsL, CtsS, Cystatin (Cst)C, Mmp2, Mmp12, Mmp14,* and *Mmp15* was determined by qPCR in WT RT2, *CtsB*$^{-/-}$*S*$^{-/-}$ RT2 and *CtsB*$^{+/-}$*S*$^{+/-}$ RT2 13.5w tumors. This analysis revealed no significant differences between genotypes with the exception of increased *Mmp15* expression in *CtsB*$^{-/-}$*S*$^{-/-}$ RT2 tumors compared to WT RT2 tumors. 3-8 independent tumors per genotype were used for analysis.

(C) mRNA expression levels of *Mmp3, Mmp9* and *Mmp13* (3 out of the 4 significantly altered genes characterized in whole tumors from WT RT2 and *CtsB*$^{-/-}$*S*$^{-/-}$ RT2 end-stage mice, see Figure 2A) was determined by qPCR analysis of bone marrow-derived macrophages (BMDMs) prepared from tumor-bearing WT RT2 and *CtsB*$^{-/-}$*S*$^{-/-}$ RT2 animals. Analysis revealed a significant decrease in

Mmp3 expression, while no significant changes in expression were detected for *Mmp9* and *Mmp13*. 3-8 independent replicates were analyzed.

(D) Tumors from WT RT2 or *CtsB*$^{-/-}$*S*$^{-/-}$ RT2 mice were sorted into a mixed population of live cells (DAPI^{-}), cancer cells (CD45^{-} CD31^{-} F4/80^{-}) or tumor-associated macrophages (TAMs) (CD45^{+} F4/80^{+} CD31^{-}). Expression of *Mmp3, Mmp9* and *Mmp13* mRNA was determined by qPCR, and the level is depicted relative to the live cell fraction. No significant changes were observed. 3-5 independent sorted samples were analyzed.

mRNA expression determined by qPCR was normalized to *Ubiquitin C* for each sample in all panels presented. Graphs show mean ± s.e.m. Statistical significance was calculated by unpaired two-tailed Student's t-test; (n.s.) nonsignificant, **P* < 0.05, ***P* < 0.01, ****P* < 0.001.

Supplemental Figure 3: Macrophage numbers and chemokine gene expression are not altered in *CtsB*$^{+/-}$*S*$^{+/-}$ tumors.

(A) Quantification of CtsZ^{+} cells in WT RT2 (*n*=62) and *CtsB*$^{-/-}$*S*$^{-/-}$ RT2 (*n*=33) tumors (as shown in Figure 4B) are plotted here with analysis of *CtsB*$^{+/-}$*S*$^{+/-}$ RT2 (*n*=32) tumors, relative to the total number of DAPI^{+} cells. This analysis showed no changes in CtsZ^{+} cell numbers in *CtsB*$^{+/-}$*S*$^{+/-}$ RT2 tumors.

(B) Quantification of Iba^{+} macrophages in WT RT2 (*n*=108) and *CtsB*$^{-/-}$*S*$^{-/-}$ RT2 (*n*=28) tumors as depicted in Figure 4C were plotted together with analysis of *CtsB*$^{+/-}$*S*$^{+/-}$ RT2 tumors (*n*=50) relative to the total number of DAPI^{+} cells. This analysis showed no changes in Iba1^{+} cells in *CtsB*$^{+/-}$*S*$^{+/-}$ RT2 tumors.

(C) mRNA expression of the macrophage marker *Cd68* was determined by qPCR analysis of WT RT2 (*n*=4) and *CtsB*$^{-/-}$*S*$^{-/-}$RT2 (*n*=6) as depicted in Figure 4D and plotted together with analysis of *CtsB*$^{+/-}$*S*$^{+/-}$ RT2 (*n*=3) tumors. This analysis showed no changes in *Cd68* expression in *CtsB*$^{+/-}$*S*$^{+/-}$ RT2 tumors, consistent with the results in (B).

(D-F) mRNA expression of the chemoattractants *Csf-1* (D)*, Ccl5* (E)*, Ccl2*, *Cxcl2*, *Cxcl14*, *Cxcl15* and *Vegf-a* (F) was determined by qPCR analysis of WT RT2, *CtsB*$^{-/-}$*S*$^{-/-}$ RT2, and *CtsB*$^{-/-}$*S*$^{-/-}$ RT2 whole tumors, and revealed a significant

increase in *Csf-1* and *Ccl5* expression in *CtsB*$^{-/-}$*S*$^{-/-}$ RT2 mice compared to their WT counterparts. All comparisons in (F) were not significant. 3-5 independent tumors per genotype were used for analysis.

mRNA expression determined by qPCR was normalized to *Ubiquitin C* for each sample in C-F. Graphs show mean ± s.e.m. Statistical significance was calculated by unpaired two-tailed Student's t-test; (n.s.) nonsignificant, **P* < 0.05, ***P* < 0.01, ****P* < 0.001.

Supplemental Figure 4: Characterization of tumorigenic phenotypes in *CtsB*$^{+/-}$*S*$^{+/-}$*Z*$^{+/-}$ RT2 and *CtsB*$^{-/-}$*S*$^{-/-}$*Z*$^{-/-}$ RT2 mice.

(A) *CtsB*$^{-/-}$*S*$^{-/-}$*Z*$^{-/-}$ RT2 and *CtsB*$^{+/-}$*S*$^{+/-}$Z$^{+/-}$ RT2 animals were generated and cumulative tumor burden, represented as the sum of the volumes of all tumors per mouse, was calculated for 13.5w WT RT2, *CtsB*$^{+/-}$*S*$^{+/-}$Z$^{+/-}$ RT2 and *CtsB*$^{-/-}$*S*$^{-/-}$Z$^{-/-}$ RT2 mice (*n*=57, *n*=18, *n*=14 mice per group, respectively).

(B) Graph depicting the average number of tumors per mouse in WT RT2, *CtsB*$^{+/-}$*S*$^{+/-}$Z$^{+/-}$ RT2 and *CtsB*$^{-/-}$*S*$^{-/-}$Z$^{-/-}$ RT2 animals at the 13.5-week endpoint. The following numbers of animals were analyzed per group: WT RT2 (*n*= 58), *CtsB*$^{+/-}$*S*$^{+/-}$Z$^{+/-}$ RT2 (*n*= 20), *CtsB*$^{-/-}$*S*$^{-/-}$Z$^{-/-}$ RT2 (*n*= 18).

(C) Graph showing the proportions of encapsulated, microinvasive and invasive carcinomas in *CtsB*$^{+/-}$*S*$^{+/-}$ RT2, *CtsB*$^{-/-}$*S*$^{-/-}$ RT2, *CtsB*$^{+/-}$*S*$^{+/-}$Z$^{+/-}$ RT2 and *CtsB*$^{-/-}$*S*$^{-/-}$Z$^{-/-}$ RT2 mice at 13.5w. The following number of mice were analyzed: WT RT2: 18 mice, 97 tumors; *CtsB*$^{+/-}$*S*$^{+/-}$ RT2: 16 mice, 98 tumors; *CtsB*$^{-/-}$*S*$^{-/-}$ RT2: 14 mice, 68 tumors; *CtsB*$^{+/-}$*S*$^{+/-}$Z$^{+/-}$ RT2: 14 mice, 49 tumors; *CtsB*$^{-/-}$*S*$^{-/-}$Z$^{-/-}$ RT2: 13 mice, 32 tumors.

(D) Quantitation of cleaved caspase-3 (CC3) staining in WT RT2, *CtsB*$^{+/-}$*S*$^{+/-}$Z$^{+/-}$ RT2, and *CtsB*$^{-/-}$*S*$^{-/-}$Z$^{-/-}$ RT2 tumors relative to the total number of DAPI^{+} cells revealed a significant 3.6-fold increase in apoptosis in tumors deficient for *CtsB, CtsS* and *CtsZ* and a 4.6-fold increase in tumors heterogygous for the three cathepsins. Tumors from 11 WT RT2, 5 *CtsB*$^{+/-}$*S*$^{+/-}$Z$^{+/-}$ RT2, and 7 *CtsB*$^{-/-}$*S*$^{-/-}$Z$^{-/-}$ RT2 mice were analyzed.

(E) Quantitation of Ki67$^+$ cells in WT RT2 (*n*= 5), *CtsB*$^{+/-}$*S*$^{+/-}$Z$^{+/-}$ RT2 (*n*= 5) and *CtsB*$^{-/-}$*S*$^{-/-}$Z$^{-/-}$ RT2 (*n*= 7) tumors relative to the total number of DAPI$^+$ cells. This analysis revealed a 53% decrease in cell proliferation in tumors deficient for *CtsB, CtsS* and *CtsZ* in combination.

(F) Quantification of CD31$^+$ endothelial cells in WT RT2 (*n*=4), *CtsB*$^{+/-}$*S*$^{+/-}$Z$^{+/-}$ RT2 (*n*=6), *CtsB*$^{-/-}$*S*$^{-/-}$Z$^{-/-}$ RT2 (*n*=10) tumors relative to the total number of DAPI$^+$ cells, as determined by immunostaining of tissue sections. This analysis revealed a significant decrease in tumor vascularization specifically in *CtsB*$^{-/-}$*S*$^{-/-}$Z$^{-/-}$ RT2 mice.

(G) Quantification of Iba$^+$ macrophages in WT RT2 (*n*=108), *CtsB*$^{-/-}$*S*$^{-/-}$ RT2 (*n*=28), *CtsB*$^{+/-}$*S*$^{+/-}$ RT2 (*n*=50), *CtsB*$^{-/-}$*S*$^{-/-}$Z$^{-/-}$ RT2 (*n*=14), *CtsB*$^{+/-}$*S*$^{+/-}$Z$^{+/-}$ RT2 (*n*=6), and *CtsZ*$^{-/-}$ RT2 (*n*=41) tumors relative to the total number of DAPI$^+$ cells. This analysis revealed that the increase in TAM numbers observed in *CtsB*$^{-/-}$*S*$^{-/-}$ RT2 tumors is lost when CtsZ is deleted in these tumors.

(H-I) mRNA expression of the chemoattractants *Csf-1* (H) and *Ccl5* (I) was determined by qPCR analysis of WT RT2 (*n*=5), *CtsB*$^{-/-}$*S*$^{-/-}$ RT2 (*n*=5), *CtsB*$^{-/-}$*S*$^{-/-}$*Z*$^{-/-}$ (*n*=4) and *Cts*$^{-}$*Z*$^{-/-}$ (*n*=5) whole tumors, which revealed a significant increase in expression of both genes in *CtsB*$^{-/-}$*S*$^{-/-}$*Z*$^{-/-}$ RT2 mice compared to WT tumors, and no changes in expression levels between *CtsB*$^{-/-}$*S*$^{-/-}$ and *CtsB*$^{-/-}$*S*$^{-/-}$*Z*$^{-/-}$ lesions. mRNA expression determined by qPCR was normalized to *Ubiquitin C* for each sample in H-I. Graphs show mean + s.e.m. Statistical significance was calculated by unpaired two-tailed Student's t-test (A, B, D-I), or using a cumulative logit model with generalized estimating equations to correct for correlations within individual mice (C); (n.s.) nonsignificant, **P* < 0.05, ***P* < 0.01, ****P* < 0.001.

Akkari, Gocheva et al, Supplemental Table 1

***CtsZ* only (*n*=9)**	***CtsZ* or any other *cathepsin* (*n*=21)**	**Any other *cathepsin* but not *CtsZ* (n=83)**
EN1%2C2.p2	DBP.p2	ADNP_IRX_SIX_ZHX.p2
FOXN1.p2	EBF1.p2	ARID5B.p2
GTF2A1%2C2.p2	ELK1%2C4_GABP{A%2CB1}.p3	BPTF.p2
HIF1A.p2	GTF2I.p2	CDX1%2C2%2C4.p2
HOX{A6%2CA7%2CB6%2CB7	HIC1.p2	CRX.p2
NFKB1_REL_RELA.p2	KLF4.p3	EP300.p2
PAX5.p2	LMO2.p2	ETS1%2C2.p2
REST.p3	MAZ.p2	EVI1.p2
TBX4%2C5.p2	MTF1.p2	EWSR1
	MYFfamily.p2	FEV.p2
	NHLH1%2C2.p2	FOX{F1%2CF2%2CJ1}.p2
	PATZ1.p2	FOXA2.p3
	RXR{A%2CB%2CG}.p2	FOXD3.p2
	SP1.p2	FOXO1%2C3%2C4.p2
	SPI1.p2	GATA1..3.p2
	SPZ1.p2	HAND1%2C2.p2
	TCF4_dimer.p2	HNF4A_NR2F1%2C2.p2
	TFAP2{A%2CC}.p2	MEF2{A%2CB%2CC%2CD}.p2
	TFAP4.p2	MYOD1.p2
	TFDP1.p2	MZF1.p2
	ZNF148.p2	NKX3
		POU5F1_SOX2{dimer}.p2
		RREB1.p2
		RUNX1..3.p2
		ZBTB16.p2
		ZNF384.p2
		AIRE.p2
		AR.p2
		ELF1%2C2%2C4.p2
		FOX{C1%2CC2}.p2
		HOX{A5%2CB5}.p2
		IKZF2.p2
		KLF12.p2
		MAFB.p2
		MYB.p2
		NFATC1..3.p2
		SI1..3.p2
		STAT2%2C4%2C6.p2
		TLX2.p2
		ALX1.p2
		DMAP1_NCOR{1%2C2}_SMARC.p2
		GFI1.p2
		GLI1..3.p2
		HES1.p2
		HMGA1%2C2.p2
		NR3C1.p2
		PITX1..3.p2
		SOX5.p2
		SRY.p2
		AHR_ARNT_ARNT2.p2
		ATF2.p2
		ATF4.p2
		bHLH_family.p2
		CEBPA%2CB_DDIT3.p2
		EGR1..3.p2
		FOSL2.p2
		FOX{I1%2CJ2}.p2
		HLF.p2
		NFE2L2.p2
		NFY{A%2CB%2CC}.p2
		NR1H4.p2
		PAX2.p2
		PAX4.p2
		POU1F1.p2
		POU3F1..4.p2
		PPARG.p2
		RBPJ.p2
		RXRA_VDR{dimer}.p2
		SOX2.p2
		SREBF1%2C2.p2
		TEAD1.p2
		TFAP2B.p2
		TFCP2.p2
		TFEB.p2
		TP53.p2
		ZFP161.p2
		HOXA9_MEIS1.p2
		LEF1_TCF7_TCF7L1%2C2.p2
		NR5A1%2C2.p2
		NR6A1.p2
		PDX1.p2
		SMAD1..7%2C9.p2
		SPIB.p2

These lists correspond to the venn diagram in Fig. 3A. The lists of transcription factor motifs (TFMs) are found in (1) the *CtsZ* promoter only, (2) *CtsZ* promoter and at least one other *cathepsin* family member (*CtsB, CtsC, CtsH, CtsL, CtsS*), or (3) absent in the *CtsZ* promoter and present in at least one of these other *cathepsin* family members. All TFM definitions can be found in the SwissRegulon database at: http://swissregulon.unibas.ch/data/mm9/mat_TF_associations.mm.